

**Supporting Information for**

**Role of geometric barriers in irregular-rupture evolution  
during the 2008 Wenchuan earthquake**

R. Okuwaki<sup>1</sup>, Y. Yagi<sup>2</sup>

<sup>1</sup> Graduate School of Life and Environmental Sciences, University of Tsukuba, Tsukuba 305-8572, Japan.

<sup>2</sup> Faculty of Life and Environmental Sciences, University of Tsukuba, Tsukuba 305-8572, Japan.

**CONTENTS**

**Figure S1.** Alternative results by using monoplane fault model.

**Figure S2.** Synthetic test of the HBP method.

**Figure S3.** Selected snapshots of Fig. 2.

**Figure S4.** Alternative results with fixed rake angle at 90°.

**Figure S5.** Histograms of rake angles weighted by signal intensity.

**Table S1.** Near-source structure used to calculate Greens functions.

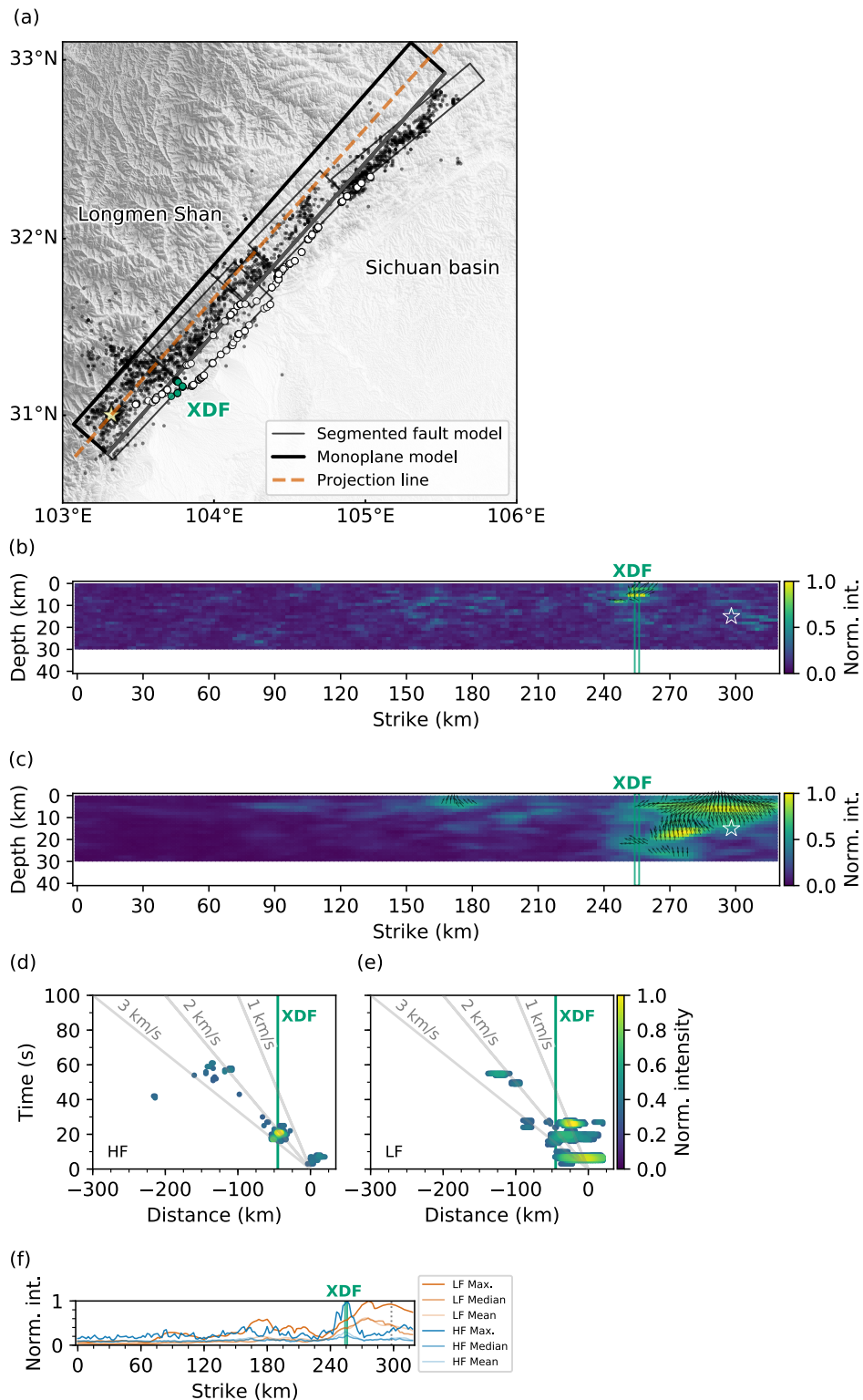


**Figure S1.** – Caption of this figure is on following page.

Alternative results by using monoplane fault model. (a) Map showing the epicenter (star), the relocated aftershocks (black dots) (Yu et al. 2010), locations of surface ruptures along the Beichuan-Pengguan segments (white circles) and the XDF (green circles) (Xu et al. 2009), the monoplane fault model (thick black rectangle) used for the validation of the main analyses (Fig. 2) and the synthetic tests of the HBP method (Fig. S2), and the segmented fault model (thin black rectangles; Fig. 1). The monoplane fault model was constructed based on the fault geometry of the SBF (Table 1) with the length of 320 km and the width of 42 km. Gray lines represent the shallowest edge of each fault segment. Orange line is the projection line drawn from the epicenter along the strike ( $221^\circ$ ) direction, used for generating Figs. 3, S1d, S1e, S2c, and S2d. Background topography is derived from 2010 Global Multi-resolution Terrain Elevation Data 7.5-arcsecond spaced mean elevations (Danielson & Gesch 2011). (b) Spatial distribution of high-frequency sources in a strike vs. depth view. Background colors represent normalized signal intensities. Arrows show rake angles, which for clarity are shown only on source cells for which signal intensities are greater than 0.5. Green lines indicate the estimated location of the XDF and the star marks the hypocenter. (c) Same as Fig. S1b, but for the low-frequency result. (d) Colored circles indicate the spatiotemporal distribution of locations of high-frequency (HF) signals along the monoplane fault model. Color scheme is the same as in Fig. 2. For clarity, only sources of normalized intensity greater than 0.3 are shown. The abscissae are distances from the epicenter along the strike ( $221^\circ$ ) direction, and the ordinate is an elapsed time from the hypocentral time. The estimated locations of the XDF (green line) and reference rupture speeds (gray lines) are also shown. (e) Same as Fig. S1d, but for the low-frequency (LF) result. (f) Distributions of maximum, median, and mean values of signal intensity along the dip direction of the monoplane fault model. The abscissae give distances along strike from the left-bottom corner of the fault model, and the ordinate is a normalized signal intensity. Cold and warm colors represent the high- and low-frequency (HF and LF) results, respectively. The estimated locations of the XDF (green lines) and the location of the hypocenter (gray dotted line) are also shown.

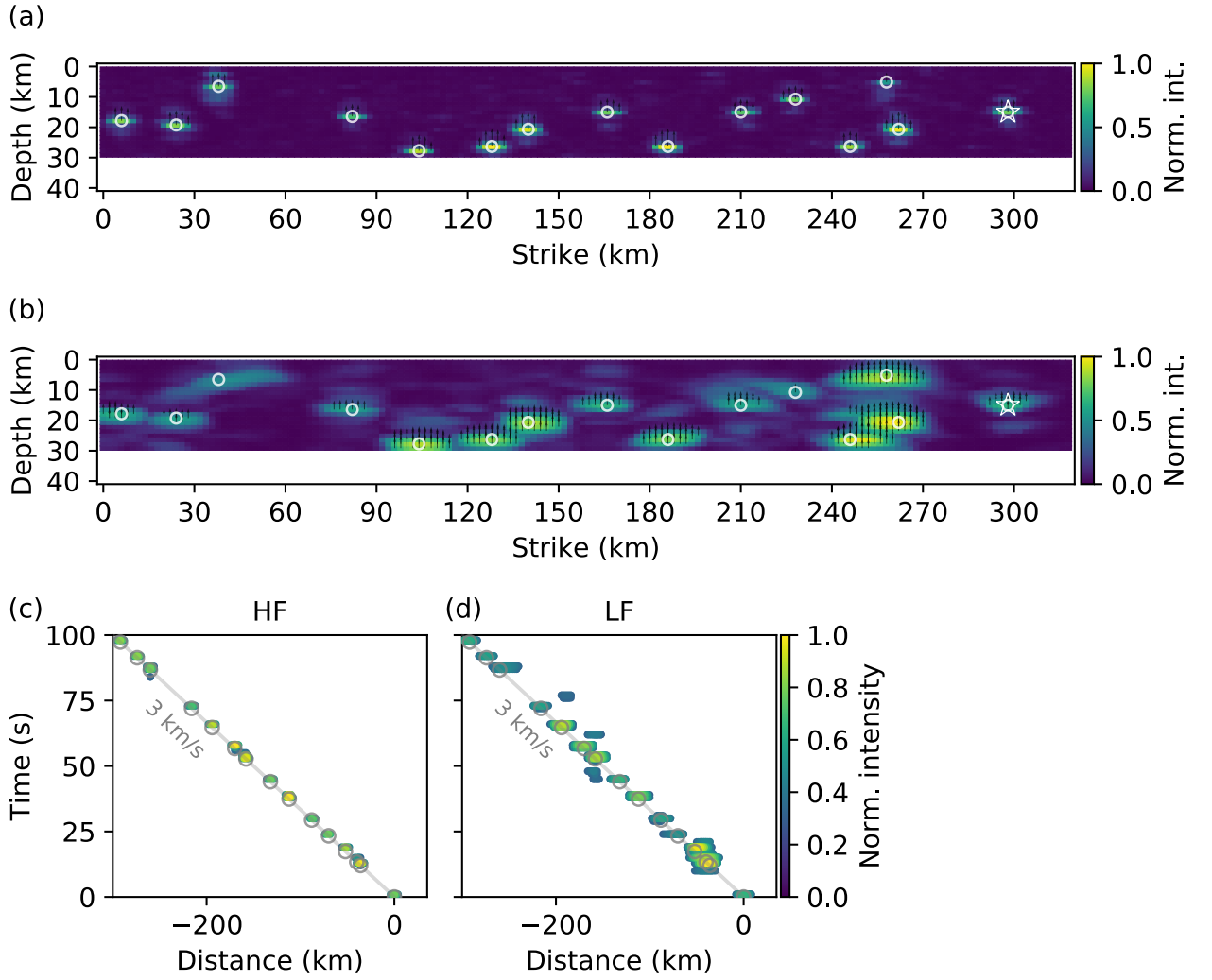


**Figure S2.** Synthetic test of the HBP method. (a) Spatial distribution of high-frequency sources in a strike vs. depth view. Background colors represent normalized signal intensities. Arrows show rake angles, which for clarity are shown only on source cells for which signal intensities are greater than 0.5. The star marks the hypocenter. We generated synthetic waveforms with multiple point sources depicted as white circles located along the monoplane fault model presented in Fig. S1. Each point source has the uniform potency generated with the rise time of 0.25 s of the triangle slip-rate function, and we assumed that each rise of the slip-rate function was triggered by the constant-propagating rupture front at 3 km/s. The Greens functions for generating the synthetic waveforms were calculated as the same procedure for the HBP analysis adopted in this study. (b) Same as Fig. S2a, but for the low-frequency result. (c) Colored circles indicate the spatiotemporal distribution of locations of high-frequency (HF) signals along the monoplane fault model. Color scheme is the same as in Fig. 2. For clarity, only sources of normalized intensity greater than 0.3 are shown. The abscissae are distances from the epicenter along the strike ( $221^\circ$ ) direction, and the ordinate is an elapsed time from initial rupture time. The locations of synthetic point sources (gray circles) and the reference rupture speed at 3 km/s (gray line) are also shown. (d) Same as figure S2c, but for the low-frequency (LF) result.

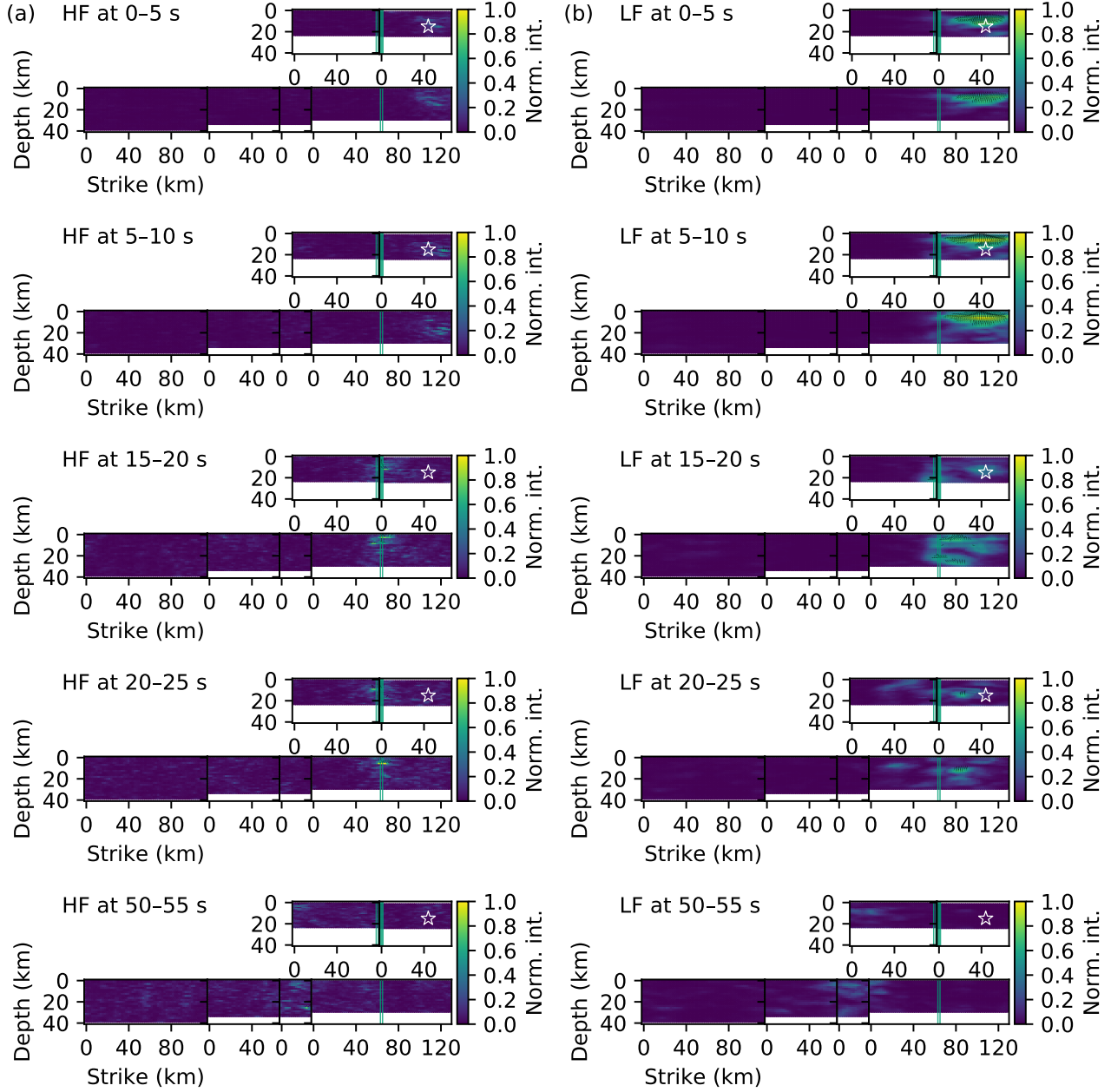


**Figure S3.** Selected snapshots of Fig. 2. (a) Selected snapshots of the high-frequency (HF) result shown in Fig. 2a taken at interval of 5 s. Background color represents the normalized signal intensity. Time range from the hypocentral time where the snapshot is taken is denoted at left-top of each panel. Layout of fault segments is the same as Fig. 2a. Arrows show rake angles, which for clarity are shown only on source cells for which signal intensities are greater than 0.5. Green lines indicate the estimated location of the XDF and the star marks the hypocenter. (b) Same as Fig. S3a, but for the low-frequency (LF) result.

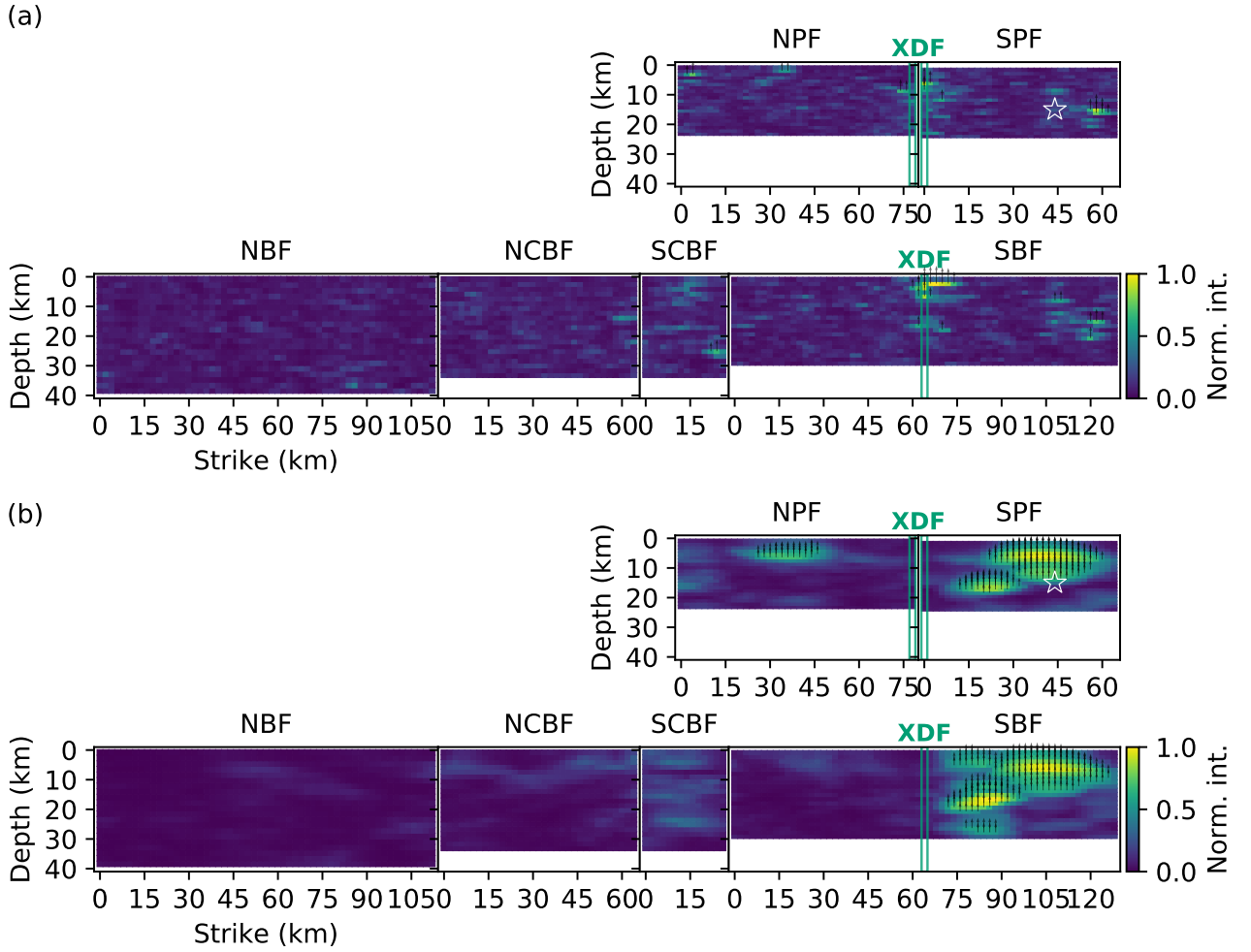


**Figure S4.** Alternative results with fixed rake angle at  $90^\circ$ . (a) Spatial distribution of high-frequency sources in a strike vs. depth view. Rake angle in Greens function is fixed at  $90^\circ$  for all the source nodes. Background colors represent normalized signal intensities. Arrows show rake angles, which for clarity are shown only on source cells for which signal intensities are greater than 0.5. Green lines indicate the estimated location of the XDF and the star marks the hypocenter. See caption of Fig. 1a for fault segment names. (b) Same as Fig. S4a, but for the low-frequency result.

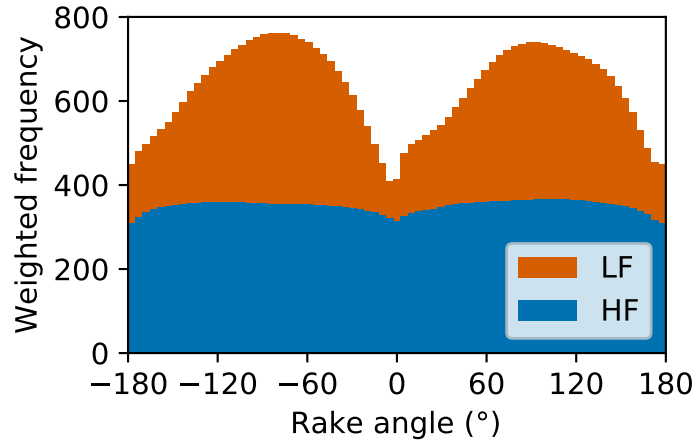


**Figure S5.** Histogram of rake angles weighted by signal intensity. The figure shows the histogram of full range of rake angles between  $-180^\circ$  and  $180^\circ$  with an increment of  $5^\circ$ . Note that the bin-count of each rake angle is weighted by its signal intensity. Blue and orange bars are the high- and low-frequency (HF and LF) results, respectively.

**Table S1.** Near-source structure used to calculate Greens functions.

$V_P$ (km/s)	$V_S$ (km/s)	Density ( $10^3 \text{kg/cm}^3$ )	Thickness (km)
4.50	2.51	2.45	4.50
5.00	2.88	2.54	2.00
6.10	3.53	2.74	11.35
6.50	3.71	2.83	12.76
6.90	3.93	2.92	21.35
8.02	4.46	3.31	0.00

## REFERENCES

- Danielson, J. & Gesch, D., 2011. Global Multi-resolution Terrain Elevation Data 2010(GMTED2010), U.S. Geol. Surv. Open-File Rep. 20111073, **2010**, 26.
- Xu, X., Wen, X., Yu, G., Chen, G., Klinger, Y., Hubbard, J., & Shaw, J., 2009. Coseismic reverse- and oblique-slip surface faulting generated by the 2008 Mw 7.9 Wenchuan earthquake, China, *Geology*, **37**(6), 515–518.
- Yu, G., Xu, X., Klinger, Y., Diao, G., Chen, G., Feng, X., Li, C., Zhu, A., Yuan, R., Guo, T., Sun, X., Tan, X., & An, Y., 2010. Fault-Scarp Features and Cascading-Rupture Model for the Mw 7.9 Wenchuan Earthquake, Eastern Tibetan Plateau, China, *Bull. Seismol. Soc. Am.*, **100**(5B), 2590–2614.